Catalytic role of enzymes: Short strong H-bond-induced partial proton shuttles and charge redistributions

Kwang S. Kim†, Kyung Seok Oh, and Jin Yong Lee

National Creative Research Initiative Center for Superfunctional Materials, Department of Chemistry, Division of Molecular and Life Sciences, Pohang University of Science and Technology, San 31, Hyojadong, Namgu, Pohang 790-784, Korea

Edited by Perry A. Frey, University of Wisconsin, Madison, WI, and approved March 27, 2000 (received for review June 29, 1999)

A two-step reaction mechanism (catalyzed alternatively by acid and base) with partial proton shuttles and charge redistributions promoted by short strong H bonds (SSHBs) (playing a dual role as an amphi-acid/base catalyst) is proposed to explain the enormous rate enhancement observed in enzymatic reactions involving carbanion intermediates. The SSHBs in the two-step reactions are found to be responsible for enhancing enzyme–substrate interactions in favor of the transition state structure over that of reactant. The detailed quantum theoretical studies of ketosteroid isomerase provide evidence of assisting roles of SSHB in enzymatic activity. The understanding of the two-step reaction mechanism would be a useful aid in designing novel functional enzymes and abzymes.

An understanding of how enzymes enhance the rate of reactions is essential for investigating the biological role of enzymes and designing new enzymes (1–3). In this context, enzyme–substrate interactions and enzyme preorganization have been invoked to explain the rate enhancement in favor of substrate transition state (TS) structures (4–14). In enzyme–substrate interactions, low barrier H bonds characterized by short and strong H bonds (SSHB) have been considered responsible for drastic enhancement in H-bond energies (4–11, 15). This concept has been introduced to explain the fast reactivities observed in various enzymes (4). Alternative explanations like preorganization in favor of the TS structures (mainly by electrostatic interactions) have also been proposed (12, 13), and the issue has been highly debated (9–24). In the present study, we attempt to resolve this issue by elucidating the origin of the catalytic role in ketosteroid isomerase (KSI), which is representative of this class of enzymes. We have carried out quantum theoretical calculations on the active sites of KSI to compare the experimental x-ray structures, NMR chemical shifts, and kinetic reaction rates for various mutants. We find evidence that the SSHB [driven by preorganized reaction environment in favor of the TS structure over the reactant structure, or enzyme–substrate complex (ES)] promotes both partial proton shuttles and (electronic) charge redistributions in a two-step mechanism as the role of an amphi-acid/base catalyst, and hence eventually leads to a drastic lowering of the activation barrier in the catalytic reaction.

KSI is one of the most proficient enzymes, catalyzing the isomerization of a variety of Δ^5-3-ketosteroids to Δ^4-3-ketosteroids (i.e., promoting an allylic rearrangement involving intramolecular proton transfer via a dienolic intermediate) (Fig. 1), with diffusion-controlled reactivity, and serves as a paradigm for fast enzymatic enolization involving carbanions (25–35). Enzyme reactions associated with carbanion intermediates responsible for isomerization reaction and carbon–carbon bond formation/cleavage are vital to metabolism of living organisms.

The important catalytic residues in *Pseudomonas testosteroni* KSI (TI) and *Pseudomonas putida* KSI (PI) have been experimentally identified: Asp-38 and Tyr-55 (TI) from the kinetic rate experiments for various mutants by Mildvan and coworkers (29–31), and Asp-99 (TI) from the NMR experiments by Pollack and coworkers (25). The x-ray structures of TI and PI and their complexes with an analogue of the reaction intermediate (equilenin) have been characterized by Oh and coworkers (32, 33). The structure of the PI complex has three key catalytic residues of Asp-40, Asp-103, and Tyr-16, and an ancillary residue Tyr-57 in proximity to equilenin. These structures are found to be essentially the same as the TI structures, wherein the corresponding catalytic residues are Asp-38, Asp-99, Tyr-14, and Tyr-55. All notations in this paper will follow PI notations for the sake of convenience. The hydroxyl group of Tyr-16 is involved in an H bonding with Tyr-57. This Tyr-16 H-bonded by Tyr-57 will be denoted as Tyr-16/57. The active site polar residues are surrounded by apolar amino acids and blocked from bulk water, resulting in zero water accessibility (32, 33). Thus, in this particular case, the hydration energy is not responsible for the catalytic activity. In addition, the x-ray structure of the equilenin complex confirms the presence of two H bonds of short distances between equilenin-O_3 (O_3) and residue-O (O_r) [$d(O_3–O_r)$: $\approx$2.6 Å for both Tyr-16 and Asp-103], implying the possible existence of SSHB (36).

The issue at hand is to explain the origin of the catalytic mechanism, i.e., on how the enzyme–substrate intermediates (EIs) and TSs are stabilized, as the reaction proceeds from ES to product (EP). The role of each catalytic residue was investigated by using *ab initio* calculations, because these theoretical approaches have been successfully used in elucidating novel interactions, properties, and reaction mechanisms (37–40).

Methods

We have carried out density functional calculations by using Becke's three parameters with Lee–Yang–Parr functionals (B3LYP) employing 6-31+G* basis set with a Gaussian 94 suite (41). Further refined energies were calculated by using Moller–Plesset second-order perturbation theory (MP2) with 6-31+G* basis set at the B3LYP/6-31+G* optimized geometries. The dielectric medium effect in the enzyme was calculated by using the self-consistent reaction field method with the dielectric constant of $\varepsilon = 18$ (31). The B3LYP and MP2 are considered to be very reliable in predicting binding energies (accuracy within a few kcal/mol), relative binding energies (within $\approx$1 kcal/mol in comparing similar systems, as systematic errors tend to cancel

This paper was submitted directly (Track II) to the PNAS office.

Abbreviations: SSHB, short strong H bond; KSI, ketosteroid isomerase; TS, transition state; ES, enzyme–substrate complex; PI, *Pseudomonas putida* KSI; TI, *Pseudomonas testosteroni* KSI; EI, enzyme–substrate intermediate; MO, molecular orbital; HOMO, highest occupied molecular orbital; MP2, Moller–Plesset second-order perturbation theory; p*A*, proton affinity; WT, wild type; B3LYP, Becke's three parameters with Lee–Yang–Parr functionals.

†To whom reprint requests should be addressed. E-mail: kim@postech.ac.kr.

The publication costs of this article were defrayed in part by page charge payment. This article must therefore be hereby marked "*advertisement*" in accordance with 18 U.S.C. §1734 solely to indicate this fact.

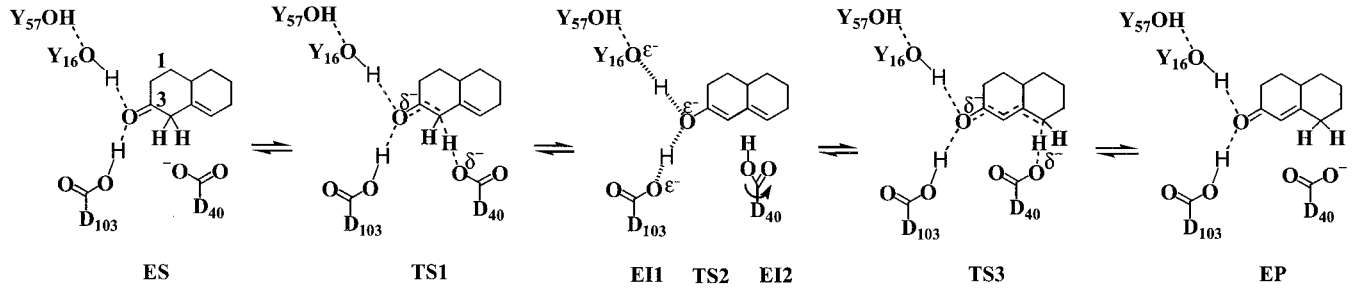

Fig. 1. Enzymatic reaction scheme of KSI.

out), and proton affinities (p*A*) (42–45). The calculated pK_a values are found to be systematically correlated to the experimental pK_a (42). In KSI, the catalytic residues are surrounded by apolar residues but not by water, and so the pK_a of the residues in the enzyme would be more similar to the p*A* values in the gas phase than the pK_a in bulk water, as seen in the experiments (the pK_a of Asp-99 in the active site of the enzyme is ≈9, whereas that in bulk water is ≈4).

To verify the reliability of our calculational results, the x-ray structure of the wild-type (WT) PI/equilenin, which imitates the reaction intermediate state, is compared with the calculated structure composed of equilenin, Asp-103, and Tyr-16/57, which were simply represented as 2-naphthol, acetic acid, and phenol H-bonded by another phenol, respectively. In calculations of the energy profiles and reaction constants, Asp-40, Asp-103, Tyr-16, Tyr-57, and steroid were simply replaced by formate, formic acid, phenol, methanol, and β,γ-enone derivative, respectively. The chemical shifts were calculated at the Hartree-Fock (HF)/6-31+G* level at the B3LYP/6-31+G* optimized geometries.

We have considered a parent system (a, parent) wherein the substrate interacts only with the anionic general base (Asp-40), and six model systems wherein the substrate interacts with Asp-40 and the following additional catalytic residues: b, Leu-103 + Phe-16; c, Asp-103; d, Tyr-16; e, Tyr-16/57; f, Asp-103 + Tyr-16; and g, Asp-103 + Tyr-16/57. These model systems can be compared, respectively, with the corresponding mutation experiments available (marked with a prime): c′, Y16F; e′, D103L or D103A; f′, Y57F; and g′, WT; in these cases, Y (Tyr) or D (Asp) was replaced by hydrophobic residue F (Phe), L (Leu), or A (Ala), which barely forms an H bond.

Results and Discussion

The structures and energies of various mutated model systems of KSI have been investigated along three reaction steps: first, abstraction of C4-β proton (ES → TS1 → EI1); second, slight rotation of protonated Asp-40 (EI1 → TS2 → EI2); and third, proton donation to C6-β position by Asp-40 (EI2 → TS3 → EP), as shown in Fig. 1. The predicted energy profile of WT (Fig. 2*A*) is similar to the corresponding experimental one of Pollack and coworkers (25). It should be noted that at TS2 the substrate is partially neutralized as the H atoms of the catalytic residues approach toward the oxyanion (O_3) in the substrate and the excess electron transfers from the substrate to the adjacent catalytic residues through the H-bonding paths. Thus, the substrate, Tyr-16/57, and Asp-103 share one negative charge unit, and their charge distributions depend on the proton affinities and electron affinities of the catalytic residues of mutants. This TS2 state with catalytic residues is contrasted to that without catalytic residues wherein the substrate is negatively charged by almost one unit.

Our calculated three-dimensional structures of EIs (complexed with equilenin instead of steroid) match almost exactly the x-ray structures of PI(g′) and TI(g′). In the predicted structure of the Tyr-16/57 + Asp-103 + equilenin complex, the two distances of $d(O_3–O_r)$ values for Tyr-16 and Asp-103 (2.54 and 2.55 Å, respectively) are in good agreement with the x-ray data (2.6 ± 0.1 Å for both in the case of PI and 2.58 ± 0.08 Å and 2.62 ± 0.07 Å, respectively, in the case of TI) (32, 33, 36). Because the calculated structures were optimized without constraints, the matching in experimental and theoretical geometries indicates that in the enzyme the key residues have almost maximal interactions with the substrate without strain.

It has been conjectured that in solution the TI active site may have the dyadic structure (Asp-99. . . Tyr-14. . . equilenin) (29), which is different from the TI and PI x-ray structures (32, 33). However, a recent NMR experiment for PI/equilenin has indicated that, in PI(D40N)/equilenin, a characteristic strong down-field resonance appears at 16.8 ppm, and a weak one at 13.1 ppm (36), similar to the case in TI/equilenin by the groups of Mildvan (29) and Pollack (25). This result is also demonstrated by our *ab initio* calculations of Tyr-16/57 + Asp-103 + equilenin complex, wherein the strong down-field resonance at 16.5 ppm is assigned to Tyr-16. The experiment also shows that, in mutant D103L + D40N, a strong down-field resonance (assigned to Tyr-16) appears, whereas in mutant Y16F + D40N the strong resonance disappears. Thus, this experiment clearly excludes the dyadic structure wherein the strong down-field resonance was assigned to Asp-103, which is H-bonded to Tyr-16 (36).

The absolute rate constants can be investigated by using the calculated activation barriers. At the B3LYP/6-31+G* and MP2/6-31+G* levels, the activation barrier of the WT of KSI is somewhat underestimated, as compared with the experimental barrier (10 to ≈11 kcal/mol) reported by Pollack and coworkers (46). However, when the dielectric medium effect of KSI (31) is taken into account, the activation barrier of the WT [at the MP2/6-31+G* level with the SCRF(B3LYP/6-31+G*; $\varepsilon = 18$)] is 8.2 kcal/mol, in close agreement with the experimental value. A slight underestimation by 2–3 kcal/mol could be explained with a more accurate calculation and a more complete model system including apolar residues around the active site. In contrast to the absolute activation barrier, the relative activation barriers between different mutants and thus the reaction mechanism are quite consistent regardless of the calculation level because of the cancellation effect between different model systems having similar environments. Thus, by using relative activation barriers between different mutants, we obtained the relative reactivity (the ratio of the kinetic rate constant of a mutant to that of the WT) or $\log(k_{cat}/k_{cat(WT)})$ with the assumption that the transfer from ES to TS1 is the rate-determining step along the reaction paths (see the footnote of Table 1). MP2 calculations reinforce the results obtained at the B3LYP level. The predicted values of $\log(k_{cat}/k_{cat(WT)})$ are in good agreement with the values measured for PI (32–35) and TI (25–28, 31) (Table 1). Given that the highly homologous three-dimensional (tertiary and quaternary) structure and the active-site environ-

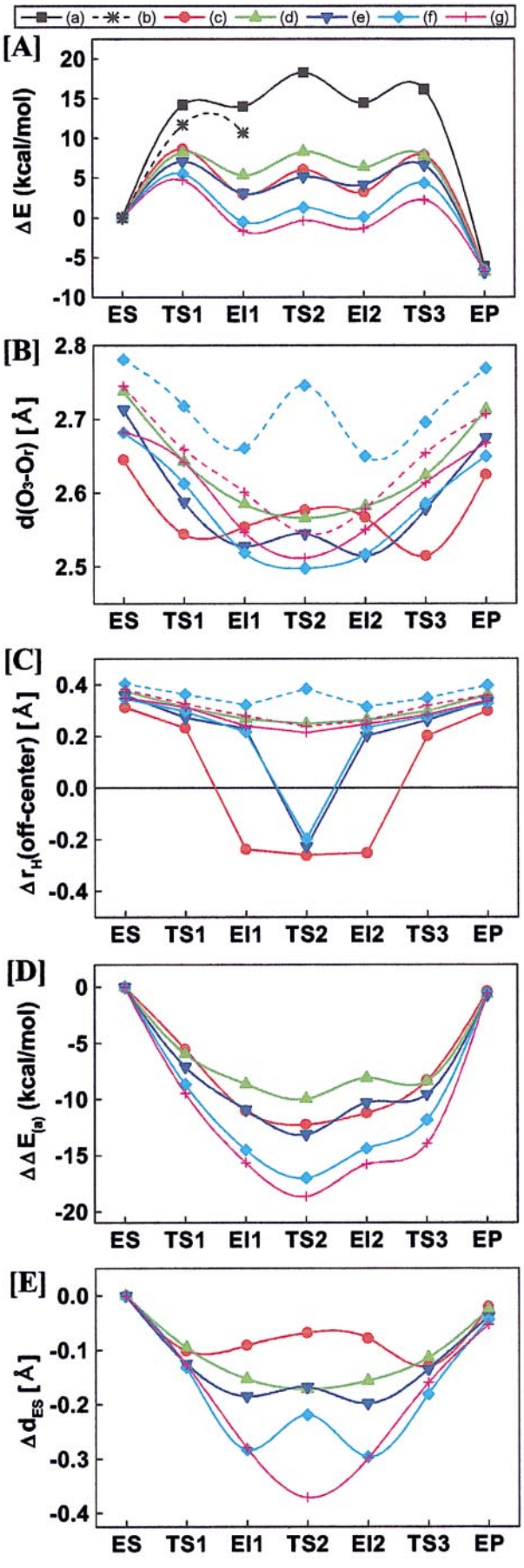

ment of TI are similar to those of PI, the catalytic reactions in the two KSIs are expected to proceed in the same way.

Fig. 2 shows the profiles of energies and H-bond distances for various mutants along the reaction path. The overall energy profiles (ΔE) (Fig. 2*A*) are almost symmetric with respect to TS2. The barriers of the first and third steps are similar. The second step, which has a small barrier (≈1 kcal/mol), cannot be rate-determining because it involves only a slight shift of the H atom through a minimal rotation (by only several degrees because Asp-40 is highly slanted against the substrate plane) about a C—C bond (or C—H bond in Figs. 1 and 3). Thus, the reaction can practically be considered to be a two-step mechanism. The residues catalyze the first step by (partially) donating a proton to the substrate (as an acid), whereas the third step is catalyzed by the (partial) acceptance of a proton from the substrate (as a base). Refer to the interoxygen distances of H bonds [$d(O_3–O_r)$ in Fig. 2*B*] and the off-center distance of a shared proton from the mid-point of O_3 and O_r [Δr_H(off-center), i.e., the degree of proton transfer in Fig. 2*C*] wherein the positive/negative value indicates that the proton is near residues/substrate.

For acidic residues with lower proton affinity (p*A* in the gas phase or pK_a in the dielectric medium), the activation barrier would be lower for the first step and higher for the third step, whereas basic residues with higher p*A* or pK_a would produce a contrary effect. Consequently, in the two-step enzyme mechanism the optimal catalytic power is obtained when the residues of the enzyme play a dual role of very strong proton donor/acceptor to/from the substrate alternatively (to be named as amphi-acid/base catalyst or proton/electron buffer) for the overall reaction. In the dielectric medium of enzymes, the maximal catalytic effect is obtained in the case of equal pK_as of residues and substrate [these pK_a values are quite different from those in bulk water]. This situation is in contrast to single-step reactions wherein a large difference in pK_a enhances the reactivity (47, 48). The condition of equal pK_as between residues and substrate for the maximal catalytic effect matches the requirement of residues in enzyme to possess equivalent pK_as with the substrate to form the maximal SSHBs (4–7, 15, 23, 24). Thus, in the two-step reaction mechanism of KSI, the SSHBs as amphi-acid/base catalysts along with partial proton shuttles and charge redistributions play a crucial role in strongly stabilizing EIs by ≈15 kcal/mol in residue-driven stabilization energy [$\Delta\Delta E_a = \Delta E - \Delta E_{parent}$ in Fig. 2*D*] and in reaction-path-dependent interoxygen distance-shortening relative to the ES state [$\Delta d_{ES} = \Sigma_r \{d(O_3–O_r) - d(O_3–O_r)_{ES}\}$ (Fig. 2*E*), i.e., shortening of $d(O_3–O_r)$s down to ≈2.5 Å by ≈0.2 Å for each].

The residue-driven stabilization energy $\Delta\Delta E_a$ is to a certain extent correlated to the Δd_{ES} unless the proton transfer occurs from the residue to the substrate (i.e., unless the Δr_H is in a negative region in Fig. 2*C*). Therefore, the stabilization at EIs and TSs can be correlated to the shortening of the H-bond distance, and hence the H-bond strength, relative to the ES state. That is, the normal (or ordinary) H bonds (between neutral partners) at ES tend to become SSHBs (involving ionic species) at EIs and TS2. Thus, these short bonds should be responsible for a portion of the residue-driven energy lowering. As for the proton transfer, the potential at ES is a single well for all mutants, whereas the potential shape (near EIs or TSs) in the

Fig. 2. Calculated energy profiles (ΔE) (*A*); interoxygen distances $d(O_3–O_r)$ (*B*); proton off-center distances ($\Delta r_{H(off\text{-}center)}$) (*C*); residue-driven energy lowering relative to the parent system ($\Delta\Delta E_a = \Delta E - \Delta E_a$) (*D*); and reaction path-dependent interoxygen distance-shortening relative to the ES state [$\Delta d_{ES} = \Sigma_r \{d(O_3–O_r) - d(O_3–O_r)_{ES}\}$, which is summed over two r's in cases f and g, whereas otherwise, over only one r] (*E*). In *B* and *C*, the dashed lines for f and g denote the second nearest residue, Tyr-16.

Table 1. Calculated activation energies ($\Delta E^{\ddagger}_{TS1}$), relative reactivities [$\log(k_{cat}/k_{cat(g)})$], and NMR chemical shifts (δ_{EI1}) for seven model systems (a–g) of KSI

Residues (mutants)	$\Delta E^{\ddagger}_{TS1}$, kcal/mol B3LYP [MP2]	$\log(k_{cat}/k_{cat(g)})$ Calc. B3LYP [MP2]	$\log(k_{cat}/k_{cat(g)})$ Exp. (PI;TI)	δ_{EI1}, ppm HF
(a) Parent	14.2 [17.0]	−6.9 [−8.2]		
(b) L103+F16 (D103L+Y16F)	11.7 [13.9]	−5.1 [−6.0]		
(c) D103 (Y16F)	8.7 [10.9]	−2.9 [−3.7]	(−3.3; −4.7)	15.1
(d) Y16	8.2 [10.7]	−2.6 [−3.6]		13.9
(e) Y16/57 (D103A, D103N)	7.1 [8.8]	−1.7 [−2.2]	(−2.1, −2.0; −3.5, −1.4)	15.1
(f) D103+Y16 (Y57F)	5.5 [6.8]	−0.6 [−0.8]	(−0.9; −0.6)	17.1
(g) D103+Y16/57 (WT)	4.7 [5.8]	0.0 [0.0]	(0.0; 0.0)	16.0

Calculated relative reactivities were compared with the PI and TI experimental values (26, 31–35). The experimental activation barrier at TS1 of WT is estimated to be 10≈11 kcal/mol by Pollack and coworkers (46). The B3LYP/6-31+G* [or MP2/6-31+G*//B3LYP/6-31+G*] predicted barriers seem to be underestimated. However, the SCRF(B3LYP/6-31+G*) correction of the dielectric medium effect ($\varepsilon = 18$) (31) is 2.4 kcal/mol. Thus, the dielectric medium effect-corrected MP2 barrier is 8.2 kcal/mol, which is close to the experimental value. Since the dielectric medium effects are similar for all mutated residues because of the similar environments, the relative reactivities are very consistent without large change in values (due to the cancellation effects), regardless of the calculation levels employed. Thus, the results are considered reliable. Furthermore, these relative reactivities are in good agreement with experimental PI and TI values. To obtain relative reactivities, k_{cat} was approximated by the reaction constant for the transition from ES to TS1, since this rate constant is the rate-determining step (see the text and Fig. 2*A*). However, in case a, the reaction constant was obtained from the activation barrier of TS2 relative to ES, because their barrier is responsible for the rate. The chemical shift δ at EI1 (δ_{EI1}) was calculated at the Hartree—Fock (HF)/6-31+G*//B3LYP/6-31+G* level.

region where Δr_H is near zero (i.e., around TS1/EI1 for c and EI1/TS2 for e and f in Fig. 2*C*) bears some characteristics of a double well. For a small absolute value of Δr_H (<≈0.5 Å) (Fig. 2*C*), the barrier for proton transfer is found to be very small in our calculation, and so the proton transfers in the double-well-type potential alone cannot explain the drastic lowering of the activation barrier. Indeed, case g, wherein the double-well-like characteristics of the potential almost disappear with little

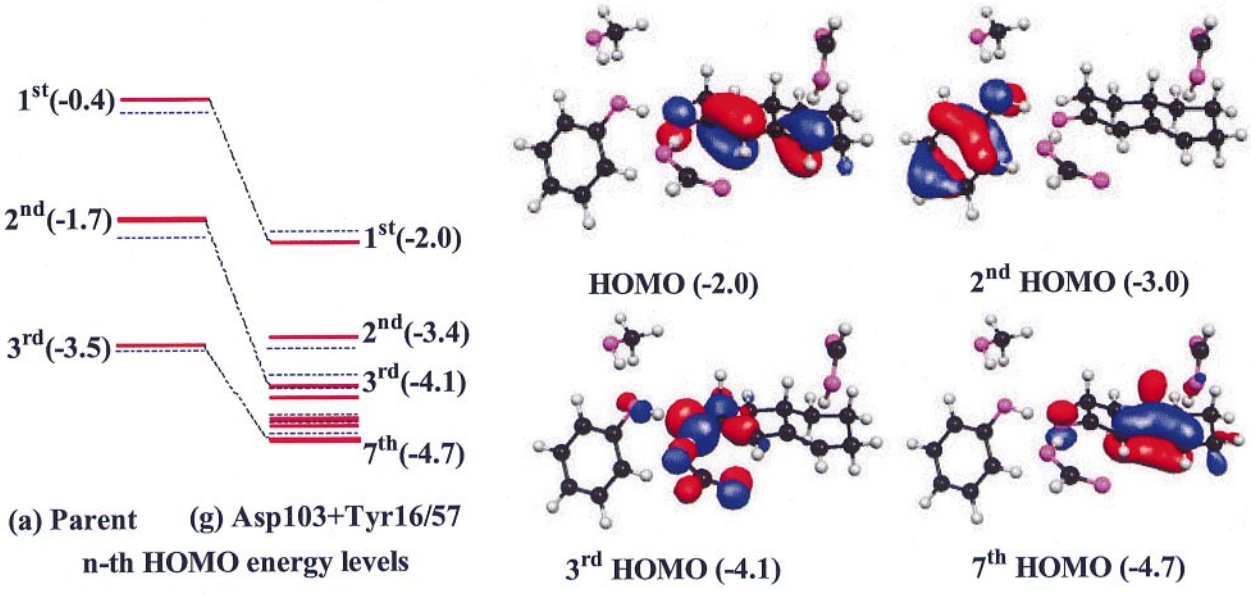

Fig. 3. Comparison of TS2 HOMOs of two model systems, (a) Parent and (g) Asp-103 + Tyr-16/57. The MO energy levels (in eV) are drawn in red and blue lines for $\varepsilon = 1$ and 10, respectively. The case for $\varepsilon = 80$ (not drawn) is similar to that for $\varepsilon = 10$. In case a, the HOMO energy of TS2 is high (−0.4 eV) compared with that of ES (−1.7 eV), because a negative charge needs to be stored in the substrate. However, the HOMO energy of ES through EP in case g is somewhat constant and highly negative (−2.0 to ≈−2.7 eV). Thus, the MOs clearly demonstrate how the catalytic residues of case g lower the activation barrier by the proton–electron rearrangements driven by SSHB compared with case a. For g, a strong π-conjugation is responsible for the change in bond orders (electron rearrangements). This π-conjugation lowers the HOMO energy drastically (−2.0 eV), because the negative charge in the substrate responsible for raising the HOMO energy of a is temporarily stored on catalytic residues Tyr-16 and Asp-103 at second to sixth HOMOs (−3.4, −4.1, −4.4, −4.6, and −4.6 eV). The seventh MO energy showing the full π-conjugation through four C atoms 3–6 (i.e., the same bond orders of 1.5 for all these carbon—carbon conjugate bonds), which is responsible for the H shift from C4 to C6 position, is also low (−4.7 eV). This low energy is in contrast to the high energy (−3.5 eV) of the corresponding MO for the full π-conjugation in case a. In the third HOMO of g, which corresponds to the second HOMO of a, the oxyanion is highly stabilized by its interaction with the H atoms of residues Tyr-16 and Asp-103. These H atoms are highly deshielded (and are therefore responsible for large chemical shifts) by two strongly electron-withdrawing O atoms of the residues, whereas each deshielded H atom (or proton) shared by both anionic O atoms shows some of the highly polarized p-like orbital characteristics (due to the sp hybridization with which the proton bridges the two O atoms). This analysis in a way reflects the characteristics of SSHBs due to MO interactions as well as noninduced electrostatic interactions.

proton transfer, shows more energy lowering than case f, which involves proton transfer in a double-well-like potential. On the other hand, it should be noted in Fig. 2 *D* and *E* that, after the proton transfers occur, the Δd_{ES} is no longer shortened but slightly lengthened, whereas the $\Delta\Delta E_a$ gets still lowered. Thus, the H-bond length shortening alone (i.e., Δd_{ES}) cannot explain the drastic barrier lowering at TSs and EIs (i.e., $\Delta\Delta E_a$). Thus, the barrier lowering at TSs and EIs needs to be explained by additional interaction forces, which will be discussed in terms of molecular orbital (MO) interactions between substrates and residues (involving charge transfer-induced electronic rearrangements or charge redistributions).

In case of two competing residues as in f and g, the cumulative stabilization of EIs/TSs results in a more enhanced k_{cat}. However, this effect is somewhat subadditive (i.e., smaller than the sum of stabilization energies of each residue) as a result of the reduced proton-withdrawing power of the oxyanion for each residue because of the presence of the other residue. This subadditivity indicates that the SSHBs would involve charge transfers and polarization (i.e., induced electrostatic interactions) and possibly partial covalent bonding. Indeed, the stabilization of EIs and TSs in the presence of catalytic residues arises mainly from the delocalization of the excess electron present in the active site by charge transfer and polarization, which will be seen below. The effective natural bond orbital population charges (49) of the substrate in cases a, c–e, and f at TS1 are -0.57, ≈ -0.43, and -0.37, respectively. Thus, the negative charge of the substrate is more reduced in the presence of two catalytic residues. This reduction arises from the transfer of the excess electron from the substrate to the catalytic residues with large electron affinity, which play the buffer role for the excess electron. Although Asp has stronger electron-withdrawing power than Tyr, Tyr has lower electron affinity than Asp. Thus, Tyr is as effective as, or slightly more effective than, Asp in lowering the activation barrier. The stabilization of the TSs and EIs in the presence of catalytic residues is highly correlated to the energy lowering of the excess electron state [to be related to the highest occupied molecular orbital (HOMO) state], as the space to accommodate the excess electron is enlarged with catalytic residues in addition to the substrate. This energy lowering is directly related to the uncertainty principle; the less localized the excess electron, the more it is stabilized.

The calculated chemical shifts (δ) are found to be somewhat correlated to the smallest value of $d(O_3–O_r)$ for the same number of H bonds [i.e., the larger δ correlates to the smaller $d(O_3–O_r)$], whereas the presence of second H bond increases δ because of the enhanced screening effect. On the basis of our results, a large value of δ can often be a good indicator of SSHB, but δ is only partly correlated to k_{cat}. This correlation particularly diminishes for large δ (>16 ppm) or small absolute value of Δr_H (<0.5 Å), as the dependence of k_{cat} on δ has been questioned (50).

The lowering of activation barriers in the presence of catalytic residues is well understood from MO analysis (Fig. 3). The striking distinction in TS2 MO energy levels between a and g arises from the quantum nature of the excess electron density accumulated on the substrate through deprotonation by Asp-40. The resulting stabilization obtained by dissipating some of the electron density to the catalytic residues is due to the uncertainty principle mentioned earlier, which is similar to what is observed in case of an excess electron interacting with water clusters (51, 52), which is in favor of a reasonably large cavity space. Thus, the presence of the catalytic residues (which play the charge buffering role by partial electron transfer from the substrate to catalytic residues) drastically reduces the charge build-up on the oxyanion. This stabilization of the EIs and TSs is essentially assisted by SSHBs. This effect is highly enhanced in the presence of both Asp-103 and Tyr-16/57. MO energies of case g are thus much lower than those in case a. The dielectric medium effect of the enzyme is not so drastic as the catalytic residue effect involving electron transfer. Thus, partial proton shuttles and charge redistributions promoted by SSHBs are more responsible for lowering of the TSs and EIs than the dielectric effect of the enzyme. Consequently, the catalytic effect results from a favorable combination of gains from noninduced electrostatic energies and MO interaction energies (polarization, charge transfer, and covalent bonding energy). Whereas the former results from the partial proton shuttles due to the presence of charged H bonds (and hence related to the SSHBs strength), the latter results mainly from electronic delocalization because of the catalytic residues, which play the buffer role for an excess electron. The MO interaction energy gain is closely related to the additional enzyme–substrate interaction promoted by SSHB.

The stabilization energy can thus be represented as the sum of the enhanced energy of the charged H bond (involving ionic species) of EIs/TSs relative to the normal H bond (between neutral partners) of the ES and the MO interaction energy gain because of the charge redistributions involving electron dissipation to the catalytic residues. Because the two energy terms are not easily separable, it is hard to estimate each term. However, we evaluate such terms in case d by using the following method. From the comparison of the energies of EI1 relative to ES in the absence and presence of Tyr-16 (Y16), the stabilization energy of EI1 by Y16 is 8.7 kcal/mol. To investigate the contribution of the noninduced electrostatic interaction (which does not include the electrostatic induction effect of the substrate + Asp-40 (D40) on the residue Y16) to the stabilization, we carried out the calculations of the ES and EI1 in the case when Y16 is replaced by a ghost residue composed of only its natural bond orbital (NBO) charges (Y16q), which were calculated for a single molecule Y16 in the absence of substrate + D40. Then, the noninduced electrostatic interaction energy gain (or preorganization-driven electrostatic energy gain) is 4.4 kcal/mol, which is responsible for enhanced bond strength of the charged H bond (i.e., SSHB itself). Then, the difference in stabilization energies between the full quantum effect by Y16 and the noninduced electrostatic effect by Y16q (4.3 kcal/mol) should come from the induced electrostatic interaction energy, covalent energy, etc. The induced electrostatic interaction includes polarization and charge transfer effects. To obtain the induced electrostatic energy gain, we first obtained the atomic charges of Y16 ($Y16q_{ind}$), which includes the induction effect in the presence of the substrate + D40. Then, we carried out the calculations of the ES and EI1 in the case when Y16 is replaced by a ghost residue ($Y16q_{ind}$) composed of its atomic point charges only. Since this stabilization energy is 8.2 kcal/mol, the induced electrostatic energy gain from the interaction between substrate + D40 and Y16 is 3.8 kcal/mol. Thus, the energy gain by the charge-transfer and polarization is large and comparable to the noninduced electrostatic energy gain. The residue Y16 plays important catalytic roles of charge buffer to withdraw and keep a large portion of the excess negative charge in the substrate as well as of the corresponding electronic charge redistribution during the reaction. This induced electrostatic energy arises from the MO interaction energy by the quantum mechanical electronic charge interaction between the catalytic residue (Y16) and the substrate + D40 (i.e., the SSHB-driven substrate–residue interaction energy). Finally, the remaining energy contribution of 0.5 (= 8.7 − 8.2) kcal/mol could correspond mostly to the nonelectrostatic covalent energy. This energy is rather small, which is further corroborated by our MO analysis that the nonelectrostatic orbital overlap in the SSHB itself is not significant.

In enzymes involving two-step reaction mechanism, a substrate is not fully negatively charged, but is partially anionic with electron dissipation to the catalytic residues. Thus, in this case the stabilization energy increment ($\approx$10 kcal/mol at EI1) driven by SSHB relative to the normal H bond turns out to be not small

[although smaller than in the case with fully negatively charged oxyanion (≈20 kcal/mol)]. If the SSHB energy is extended to include the substrate–residue interactions due to charge redistributions in both substrate and residue, it is the stabilization energy that is the sum of the preorganization-driven SSHB energy and the SSHB-driven MO interaction energy. However, if we consider only the strength of the SSHB itself, the binding energy increment [relative to the normal H bond whose binding energy is ≈5 kcal/mol (53)] is much reduced (to ≈5 kcal/mol).

Conclusions

This study presents evidence of the role of SSHB in driving partial proton shuttles and charge redistributions in a real enzyme system (KSI). A large stabilization energy for EIs/TSs relative to ES comes from both the enhanced H-bond energy (of SSHBs relative to normal H bonds) and the MO interaction energy (by the electronic charge redistributions due to charge transfers and polarization involving excess electron dissipation to the catalytic residues and possibly by partial covalent bonding). Thus, it can be said that the activation barrier is lowered predominantly by both preorganization-driven SSHB and SSHB-driven proton shuttles and charge redistributions. The origin of the catalytic role of SSHB is explained with a dual role of very strong proton donor/acceptor to/from substrate in catalytic activation involved in two-step reactions to be catalyzed alternatively by acid and base. This understanding would help open up a new avenue for designing novel enzymes and antibodies acting through this mechanism.

We thank Professors K. Y. Choi and B. H. Oh for providing us their x-ray structures and mutation experimental data of KSI. We also thank Professors S. J. Benkovic, J. Chin, W. W. Cleland, D. Herschlag, A. S. Mildvan, R. M. Pollack, and anonymous referees for their critical reviews of the manuscript. This work was supported by Creative Research Initiatives of the Korean Ministry of Science and Technology.

1. Kirby, A. J. (1996) *Angew. Chem. Int. Ed. Engl.* **35,** 707–724.
2. Stewart, J. D. & Benkovic, S. J. (1995) *Nature (London)* **375,** 388–391.
3. Mesecar, A. D., Stoddard, B. L. & Koshland, D. E. (1997) *Science* **277,** 202–206.
4. Cleland, W. W. & Kreevoy, M. M. (1994) *Science* **264,** 1887–1890.
5. Cleland, W. W. (1992) *Biochemistry* **31,** 317–319.
6. Gerlt, J. A. & Grassman, P. G. (1993) *Biochemistry* **32,** 11943–11952.
7. Gerlt, J. A. & Grassman, P. G. (1993) *J. Am. Chem. Soc.* **115,** 11552–11568.
8. Frey, P. A., Whitt, S. A. & Tobin, J. B. (1994) *Science* **264,** 1927–1930.
9. Lin, J., Westler, W. M., Cleland, W. W., Markely, J. L. & Frey, P. A. (1998) *Proc. Natl. Acad. Sci. USA* **95,** 14664–14668.
10. Zheng, Y.-J. & Bruice, T. C. (1997) *Proc. Natl. Acad. Sci. USA* **94,** 4285–4288.
11. Schiott, B., Iversen, B. B., Madsen, G. K. H., Larsen, F. K. & Bruice, T. C. (1998) *Proc. Natl. Acad. Sci. USA* **95,** 12799–12802.
12. Cannon, W. R., Singleton, S. F. & Benkovic, S. J. (1996) *Nat. Struct. Biol.* **3,** 821–833.
13. Warshel, A. (1998) *J. Biol. Chem.* **273,** 27035–27038.
14. Warshel, A. Papazyan, A. & Kollman, P. A. (1995) *Science* **269,** 102–103.
15. Perrin, C. L. & Nielson, J. B. (1997) *Annu. Rev. Phys. Chem.* **48,** 511–544.
16. Gurthrie, J. P. (1996) *Chem. Biol.* **3,** 163–170.
17. Ash, E. L., Sudmeier, J. L., De Fabo, E. C. & Bachovchin, W. W. (1997) *Science* **278,** 1128–1132.
18. Cannon, W. R. & Benkovic, S. J. (1998) *J. Biol. Chem.* **273,** 26257–26260.
19. Cleland, W. W., Frey, P. A. & Gerlt, J. A. (1998) *J. Biol. Chem.* **273,** 25529–25532.
20. Cleland, W. W. & Kreevoy, M. M. (1995) *Science* **269,** 104.
21. Frey, P. A. (1995) *Science* **269,** 104–106.
22. Gerlt, J. A., Kreevoy, M. M., Cleland, W. W. & Frey, P. A. (1997) *Chem. Biol.* **4,** 259–267.
23. Shan, S., Loh, S. & Herschlag, D. (1996) *Science* **272,** 97–101.
24. Shan, S. & Herschlag, D. (1996) *Proc. Natl. Acad. Sci. USA* **93,** 14474–14479.
25. Wu, Z. R., Ebrahimian, S., Zawrotny, M. E., Thornburg, L. D., Perez-Alvarado, G. C., Brothers, P., Pollack, R. M. & Summers, M. F. (1997) *Science* **276,** 415–418.
26. Thornburg, L. D., Henot, F., Bash, D. P., Hawkinson, D. C., Bartel, S. D. & Pollack, R. M. (1998) *Biochemistry* **37,** 10499–10506.
27. Hawkinson, D. C., Pollack, R. M. & Ambulos, N. P. (1994) *Biochemistry* **33,** 12172–12183.
28. Hawkinson, D. C. & Pollack, R. M. (1993) *Biochemistry* **32,** 694–698.
29. Zhao, Q., Abeygunawardana, C., Gittis, A. G. & Mildvan, A. S. (1997) *Biochemistry* **36,** 14616–14626.
30. Zhao, Q., Abeygunawardana, C., Talalay, P. & Mildvan, A. S. (1996) *Proc. Natl. Acad. Sci. USA* **93,** 8220–8224.
31. Li, Y.-K., Kuliopulos, A., Mildvan, A. S. & Talalay, P. (1993) *Biochemistry* **32,** 1816–1824.
32. Kim, S. W., Cha, S.-S., Cho, H.-S., Kim, J.-S., Ha, N.-C., Cho, M.-J., Joo, S., Kim, K. K., Choi, K. Y. & Oh, B.-H. (1997) *Biochemistry* **36,** 14030–14036.
33. Cho, H.-S., Choi, G., Choi, K. Y. & Oh, B.-H. (1998) *Biochemistry* **37,** 8325–8330.
34. Kim, S. W., Joo, S., Choi, G., Cho, H.-S., Oh, B.-H. & Choi, K. Y. (1997) *J. Bacteriol.* **179,** 7742–7747.
35. Kim, S. W. & Choi, K. W. (1995) *J. Bacteriol.* **177,** 2602–2605.
36. Cho, H.-S., Ha, N.-C., Choi, G., Kim, H.-J., Lee, D., Oh, K. S., Kim, K. S., Lee, W., Choi, K. Y. & Oh, B. H. (1999) *J. Biol. Chem.* **274,** 32863–32868.
37. Choi, H. S., Suh, S. B., Cho, S. J. & Kim, K. S. (1998) *Proc. Natl. Acad. Sci. USA* **95,** 12094–12099.
38. Kim, K. S., Lee, J. Y., Lee, S. J., Ha, T.-K. & Kim, D. H. (1994) *J. Am. Chem. Soc.* **116,** 7399–7400.
39. Kim, K. S., Kim, B. H., Park, W. M., Cho, S. J. & Mhin, B. J. (1993) *J. Am. Chem. Soc.* **115,** 7472–7477.
40. Choi, H. S. & Kim, K. S. (1999) *Angew. Chem. Int. Ed.* **38,** 2256–2258; *Angew. Chem.* **111**, 2400–2402 (German).
41. Frisch, M. J., Trucks, G. W., Schlegel, H. B., Gill, P. M. W., Johnson, B. G., Robb, M. A., Cheeseman, J. R., Keith, T. A., Petersson, G. A., Montgomery, J. A., *et al.* (1995) *Gaussian 94* (Gaussian, Pittsburgh, PA).
42. Hehre, W. J., Radom, L., Schleyer, P. v. R. & Pople, J. A. *Ab Initio Molecular Orbital Theory* (1986) Wiley, New York.
43. Curtiss, L. A., Raghavachari, K., Redfern, P. C. & Pople, J. A. (1997) *J. Chem. Phys.* **106,** 1063–1079.
44. Kim, J. & Kim, K. S. (1998) *J. Chem. Phys.* **109,** 5886–5895.
45. Bash, P. A., Field, M. J., Davenport, R. C., Oetsko, G. A., Ringe, D. & Karplus, M. (1991) *Biochemistry* **30,** 5826–5832.
46. Hawkinson, D. C., Eames, T. C. M. & Pollack, R. M. (1991) *Biochemistry* **30,** 10849–10858.
47. Smith, D. M., Golding, B. T. & Radom, L. (1999) *J. Am. Chem. Soc.* **121,** 1383–1384.
48. Chen, J., McAllister, M. A., Lee, J. K. & Houk, K. N. (1998) *J. Org. Chem.* **63,** 4611–4619.
49. Reed, A. E., Curtiss, L. A. & Weinhold, F. (1988) *Chem. Rev.* **88,** 899–920.
50. Garcia-Viloca, M., Gelabert, R., Gonzalez-Lafont, A., Moreno, M. & Lluch, J. M. (1997) *J. Phys. Chem. A* **101,** 8727–8733.
51. Lee, S., Kim, J., Lee, S. J. & Kim, K. S. (1997) *Phys. Rev. Lett.* **79,** 2038–2041.
52. Kim, K. S., Lee, S., Kim, J. & Lee, J. Y. (1997) *J. Am. Chem. Soc.* **119,** 9329–9330.
53. Kim, K. S., Mhin, B. J., Choi, U.-S. & Lee, K. (1992) *J. Chem. Phys.* **97,** 6649–6662.